$Ba_2Mn_2O_4Cu_{0.9}S$: A layered Oxysulfide with a New Perovskite-Related Manganese Oxide Fragment

Geoffrey Hyett, Zoltán A. Gál, Catherine F. Smura, and Simon J. Clarke*

Inorganic Chemistry Laboratory, Department of Chemistry, University of Oxford, South Parks Road, Oxford OX1 3QR, United Kingdom

Received July 30, 2007. Revised Manuscript Received October 19, 2007

The oxysulfides $Ba_2Mn_2O_4Cu_{0.9}S$ and $Ba_{1.3}Sr_{0.7}Mn_2O_4CuS$ are reported. The compounds crystallize in space group *P*4/*nmm* with 2 formula units in the unit cell and lattice parameters $a = 3.9916(1)$ Å and $c = 19.5628(5)$ Å for a refined composition of $Ba_2Mn_2O_4Cu_{0.89(1)}S$ and $a = 3.9595(1)$ Å and $c = 19.2227(3)$ Å for $Ba_{1.32(3)}Sr_{0.68(4)}Mn_2O_4Cu_{0.98(2)}S$ determined, respectively, from powder neutron and X-ray single-crystal diffraction measurements. The structure consists of alkaline earth Manganite slabs composed of MnO_5 square-based pyramids sharing edges and vertexes, which are separated by CuS antifluorite-type puckered layers. The central part of the alkaline earth manganite slab is composed of MnO_5 square-based pyramidal units sharing all four of their basal edges with neighboring units in the basal plane and sharing their apical vertices with those of square-based MnO_5 pyramids in the outer part of the alkaline earth manganite slab. This is similar to a structural fragment in the as-yet-unrealized strontium iron oxide $Sr_4Fe_6O_{12}$, which is the oxide-poor relative of the anion-conducting $Sr_4Fe_6O_{13\pm\delta}$ phases. The intrinsic copper deficiency in semiconducting $Ba_2Mn_2O_4Cu_{0.9}S$ suggests a mean manganese oxidation state of +2.55. The results of magnetic susceptibility measurements and low-temperature neutron diffraction results suggest that some moments participate in long-range antiferromagnetic order, whereas others give rise to spin-glass-like behavior.

Introduction

Perovskites with general formula AMX_3 in which A is usually an electropositive metal cation, M is usually a transition or main group metal cation, and X is usually the oxide anion, and related compounds are of great importance in solid-state chemistry and technology. Perovskites are extremely tolerant of ionic substitution at all the crystallographic sites, resulting in a wide array of physical properties. Derivatives of cubic perovskites such as the Ruddlesden–Popper (R–P) phases $A_{n+1}M_nX_{3n+1}$,[1] for which n is usually ≤ 3 and for which the $n = \infty$ member is perovskite itself, are also important and have received much attention in recent years, particularly in the context of the high-temperature cuprate superconductors and the magnetoresistive manganites. The R–P phases may be considered intergrowths of blocks of the cubic perovskite structure n layers of octahedra thick separated by AX layers that resemble slabs of the rock-salt structure. Recently, a number of more complex intergrowth phases have been isolated in which perovskite-type oxide blocks are separated by antifluorite-type slabs $M'_{2m}E_m+1$ ($m = 1, 2, 3$) in which M' is usually a late transition metal or a main group metal and is tetrahedrally coordinated by a nonoxide anion E, which is usually a chalcogenide[2–6] or pnictide[7] anion. These phases are most widely represented by oxychalcogenides in which the antifluorite layer is composed of Cu^+ ions in tetrahedral coordination by chalcogenide anions. References 2−6 describe and illustrate the structures of a wide range of layered oxychalcogenide phases. These compounds show a similarly wide range of properties to that displayed by pure oxides. Because the synthetic conditions for these chalcogenide or pnictide-containing phases must be anaerobic, and because the chalcogens and pnictogens are less oxidizing than oxygen, lower transition metal oxidation states may be stabilized in the mixed-anion phases than are commonly found in pure oxide analogues. For example, the oxychalcogenides $Sr_4Mn_3O_{7.5}Cu_2Ch_2$ (Ch = S, Se)[2,7] contain Mn^{3+} ions resulting in anion-deficiency, whereas oxidation states as high as +4 for Mn may readily be obtained in pure oxide Manganite perovskite and R−P phases. In this paper, we report two examples of the new oxysulfide $Ba_{2-x}Sr_xMn_2O_4Cu_{1-\delta}S$ ($x = 0$, 0.7; $\delta = 0.1$ for $x = 0$) that contain Mn in an oxidation state close to +2.5 and a novel perovskite-related oxide slab composed of edge- and vertex-sharing MnO_5 square-based pyramids that resembles a structural fragment predicted in the idealized structure of the perovskite relative $Sr_2Fe_3O_6$ (= $Sr_4Fe_6O_{12}$),[9] but realized only imperfectly in the oxide-rich relatives of that idealized phase: $Sr_4Fe_6O_{13\pm\delta}$,[10] which has been revealed as an important mixed electronic and oxide ion conductor. The structure and magnetic and transport properties of $Ba_2Mn_2O_4Cu_{0.9}S$ are reported.

Experimental Section

Synthesis. The products reported are air stable; however, one or more moisture-sensitive reactants was invariably involved, so

* E-mail: simon.clarke@chem.ox.ac.uk. Fax: 44 1865 272690. Tel: 44 1865 272600.

(1) Ruddlesden, S. N.; Popper, P. *Acta Crystallogr.* **1958**, *11*, 54.
(2) Zhu, W. J.; Hor, P. H. *J. Solid State Chem.* **2000**, *153*, 26.
(3) Zhu, W. J.; Hor, P. H.; Jacobson, A. J.; Crisci, G.; Albright, T. A.; Wang, S.-H.; Vogt, T. *J. Am. Chem. Soc.* **1997**, *119*, 12398.
(4) Zhu, W. J.; Hor, P. H. *J. Solid State Chem.* **1997**, *130*, 319.
(5) Gál, Z. A.; Rutt, O. J.; Smura, C. F.; Overton, T. P.; Barrier, N.; Clarke, S. J.; Hadermann, J. *J. Am. Chem. Soc.* **2006**, *128*, 8530.
(6) Zhu, W. J.; Hor, P. H. *J. Solid State Chem.* **1997**, *134*, 128.
(7) Brock, S. L.; Raju, N. P.; Greedan, J. E.; Kauzlarich, S. M. *J. Alloys Compd.* **1996**, *237*, 9.
(8) Hyett, G.; Barrier, N.; Clarke, S. J.; Hadermann, J. *J. Am. Chem. Soc.* **2007**, *129*, 11192.
(9) Rossell, M. D.; Abakumov, A. M.; Van Tendeloo, G.; Lomakov, M. V.; Istomin S., Ya.; Antipov, E. V *Chem. Mater.* **2005**, *17*, 4717.

10.1021/cm7021054 CCC: $40.75
Published on Web 12/27/2007

manipulations of solids were carried out in a glove box technology dry box containing recirculated argon with a combined O_2 and H_2O content of less than 5 ppm. The following starting materials were used as supplied: MnO_2 powder (ALFA 99.999%), Cu powder (ALFA 99.9995%), Mn flake (Aldrich 99.98%) cleaned with 15% nitric acid in methanol and ground into powder in the dry box, and CuO powder (ALFA 99.9999%). BaS and SrS were synthesized by the reaction at 900 °C for 8 h between $BaCO_3$ (ALFA 99.99%) or $SrCO_3$ (ALFA 99.994%) powders and CS_2 (Aldrich 99.5%) vapor that was carried over the hot carbonate by a stream of argon (BOC, Pureshield) (**Caution:** *CS_2 is toxic and highly flammable: the apparatus was contained in a fume hood and excess CS_2 was destroyed by bubbling the exhaust gases through hydroxide bleach*). Cu_2S was prepared by reacting copper powder with sulfur (ALFA 99.9995%) in a dried evacuated sealed silica tube at 700 °C for 3 days. The temperature was slowly raised between 400 and 700 °C after a 12 h soak at 400 °C in order to avoid a buildup of sulfur pressure. SrO was prepared by decomposing $SrCO_3$ under a dynamic vacuum at 900 °C for 24 h with a final firing of 3 h at 1100 °C. BaO was prepared in a similar way: with two firings under a vacuum at 950 °C to decompose most of the carbonate, followed by a final firing at 1100 °C.

In the synthesis of each of the products, the reactants were mixed thoroughly in an agate pestle and mortar, pressed into a pellet at 150 MPa, and placed in a dry alumina crucible inside a silica tube that had been baked dry under a vacuum for 2–3 h at 1000 °C prior to loading in the dry box. The tube was sealed under vacuum (1×10^{-2} mbar) and heated in an electrical resistance chamber furnace. The first sample of the new material described in this paper was $Ba_{1.3}Sr_{0.7}Mn_2O_4CuS$ obtained as single crystals in a reaction with the intended target $Ba_{2.5}Sr_{1.5}Mn_3O_{7.5}Cu_2S_2$ (a relative of the previously reported $Sr_4Mn_3O_{7.5}Cu_2Ch_2$ (Ch = S, Se) phases[2,8]). In this synthesis, BaS, BaO, SrO, Mn, MnO_2, and Cu_2S were reacted together in the molar ratio 1:1.5:1.5:0.75:2.25:1 at 1200 °C for 24 h and then cooled at 0.2 °C min^{-1}. After identification of the phase $Ba_{1.3}Sr_{0.7}Mn_2O_4CuS$ with a new structure type from this reaction, an attempt was made to synthesize the analogue containing only Ba^{2+} as the alkaline earth cation. A sample with the composition $Ba_2Mn_2O_4CuS$ (sample A) was obtained as a bulk powder on the 4 g scale by reacting together equimolar quantities of BaS, BaO, CuO, MnO_2, and Mn powders at 900 °C for 10 days followed by cooling at 5 K min^{-1}. Subsequent neutron diffraction measurements on this sample that are described below revealed that the strontium-free oxysulfide has an intrinsic copper deficiency of about 10% (i.e., sample A is intrinsically multiphase, containing the oxysulfide and elemental copper), and in subsequent syntheses of material for physical property measurements, the molar ratios were adjusted so as to avoid the presence of surplus elemental copper in the product. Material of composition $Ba_2Mn_2O_4Cu_{0.9}S$ (sample B) was obtained by reacting together BaS, BaO (99.99%, Aldrich), CuO, MnO_2, and Mn (Aldrich 99.99%) powders in the molar ratio 1:1:0.9:1.05:0.95. The pellet of material was heated at 900 °C for periods of 10 days and 2 days with regrinding between heating cycles. Cooling was always carried out at a rate of 5 K min^{-1} to avoid competition from $Ba_4Mn_3O_{7.5}Cu_2S_2$.

Chemical Analysis. Analysis was carried out using a JEOL JSM-840A scanning electron microscope equipped with an Oxford Instruments ISIS300 energy-dispersive X-ray (EDX) analysis system on the same crystal of $Ba_{1.3}Sr_{0.7}Mn_2O_4CuS$ as was used in the single-crystal X-ray diffraction measurement. The elemental content was determined from nine different spots on the crystal.

Single-Crystal X-ray Dffraction. Intensity data for a black single crystal ($0.05 \times 0.05 \times 0.04$ mm^3) of $Ba_{1.3}Sr_{0.7}Mn_2O_4CuS$ were collected on a Nonius Kappa CCD diffractometer using graphite-monochromated Mo $K\alpha$ radiation ($\lambda = 0.71073$ Å) at room temperature. The frames were recorded using $\Delta\omega = 1.20°$ rotation scans with an X-ray exposure time of 100 s per frame. Reflection indexing, Lorentz-polarization correction, peak integration, and background determination were performed using the program DENZO[11] of the Kappa CCD software package. A numerical absorption correction based on face-indexing[12] was applied to the reflection intensities. Structure solution using the Patterson method and structure refinement were carried out using the SHELXL97[13] suite via the WinGX interface.[14]

Neutron Powder Diffraction. Measurements were performed at room temperature and 2 K on the high-resolution powder diffractometer, HRPD at the ISIS facility, Rutherford Appleton Laboratory, U.K. Three and a half grams of sample A contained in a cylindrical vanadium container was measured for 3 h for a normalized integrated proton current at the production target of 100 μA h. ZnS scintillator detectors at mean scattering angles 2θ of 165 and 90° and a low-angle ($2\theta = 30°$) detector (^{3}He tube) gave usable data covering the d-spacing range $0.7 < d < 7$ Å at a resolution $\Delta d/d$ of about 1×10^{-3}. An orange cryostat was used for the low-temperature measurement. Further room-temperature measurements were made on the same sample using the POLARIS diffractometer at ISIS enabling a wider d-spacing coverage in this case ($0.3 < d < 8$ Å) via detectors at scattering angles of 145° (^{3}He tubes), 90° (ZnS scintillator), and 35° (^{3}He tubes).

X-ray Powder Diffraction. Measurements to assess phase purity were performed on a Panalytical X'Pert PRO diffractometer equipped with an X'Celerator detector using Cu $K\alpha_1$ radiation selected using a Ge(111) monochromator.

Magnetometry. Measurements were carried out using a Quantum Design MPMS-XL SQUID magnetometer in the temperature range 5−300 K and at magnetic fields of up to 5 T. Seventy-six milligrams of sample A and 45 mg of Sample B were contained in gelatin capsules. Measurements of the susceptibility were made on warming in a measuring field of 100 mT after cooling in zero field (zero-field-cooled, ZFC) and then again on warming after cooling in the measuring field (field-cooled, FC). Hysteresis measurements were made after cooling from 300 K in the maximum field (5 T) and then measuring a full magnetization isotherm in the range ±5 T.

Electrical Conductivity Measurements. Measurements were performed on sample B using the four-probe method using a homemade apparatus.

Results and Discussion

Synthesis and Crystal Structure. The reaction intended to produce single crystals of $Ba_{2.5}Sr_{1.5}Mn_3O_{7.5}Cu_2S_2$ as part of the exploration of the solid solution $Ba_{4-x}Sr_xMn_3O_{7.5}Cu_2S_2$ did produce crystals of the target phase,[15] but also produced crystals with a primitive tetragonal cell of dimensions a = 3.9595(1) Å and c = 19.2227(3) Å that did not match any known phase in the ICSD database.[16] EDX analysis on the crystal yielded a Ba:Sr:Mn:Cu:S ratio of 1.11(1):0.61(1):1.81(2):0.91(1):1.00(2); this information was used in the

(10) Kanamura, F.; Shimada, M.; Koizumi, M. *J. Phys. Chem. Solids* **1972**, *33*, 1169.
(11) Otwinowski, Z.; Minor, W. DENZO-SMN. In *Methods in Enzymology, Macromolecular Crystallography, Part A*; Carter, C. W., Jr., Sweets, R. M., Eds.; Academic Press: New York,1997; Vol. 276.
(12) Alcock, N. W. *Crystallogr. Computing* **1970**, 271.
(13) Sheldrick, G. M. *SHELX97: Programs for Crystal Structure Analysis (Release 97–2)*; University of Göttingen: Göttingen, Germany, 1997.
(14) Farrugia, L. J. *J. Appl. Crystallogr.* **1999**, *32*, 837.
(15) Hyett, G. PhD Thesis, University of Oxford, Oxford, U.K., 2006.

Table 1. Results of Refinements of the Structures of $Ba_{1.3}Sr_{0.7}Mn_2O_4CuS$ and $Ba_2Mn_2O_4Cu_{0.9}S$ Against SXRD and PND Data, Respectively

formula	$Ba_{1.3}Sr_{0.7}Mn_2O_4CuS$	$Ba_2Mn_2O_4Cu_{0.9}S$	
refined composition	$Ba_{1.32(3)}Sr_{0.68(4)}Mn_2O_4Cu_{0.98(1)}S$	$Ba_2Mn_2O_4Cu_{0.89(1)}S$	
radiation	Mo $K\alpha$, $\lambda = 0.71073$ Å	neutron ToF	
instrument	Enraf Nonius FR590 κCCD	HRPD	
physical form	black prism	black powder	
T (K)	240	298	2
cryst syst	tetragonal		
space group	$P4/nmm$ (No. 129)		
fw	509.07	537.73	537.73
a (Å)	3.9595(1)	3.99181(7)	3.98297(1)
c (Å)	19.2227(3)	19.5641(3)	19.4758(1)
V (Å^3)	301.37(1)	311.75(1)	308.966(2)
Z	2	2	2
ρ_{calcd} (mg m^{-3})	5.61	5.73	5.78
no. of independent reflns	395		
no. of variables	33	75	48
χ^2	1.281	5.087	12.31
R_1	0.0213		
wR_2	0.0527		
R_p		0.0547	0.0523
wR_p		0.0395	0.0492
$R(F^2)$		0.091	0.15

Table 2. Refined Atomic Positions for $Ba_{1.3}Sr_{0.7}Mn_2O_4CuS$ in $P4/nmm$[a] from SXRD Data at 240 K

atom	site	x	y	z	U(eq)[b] (Å^2) × 100	occupancy
Mn1	2c	¼	¼	0.46633(4)	0.84(3)	1[c]
Mn2	2c	¼	¼	0.25411(5)	0.64(3)	1[c]
Ba1/Sr1	2c	¾	¾	0.34918(2)	1.00(2)	0.84(2) (Ba)[d]
Ba2/Sr2	2c	¾	¾	0.15183(2)	0.75(2)	0.48(2) (Ba)[d]
O1	4f	¼	¾	0.24145(2)	1.09(7)	1[c]
O2	2c	¼	¼	0.3618(3)	1.6(1)	1[c]
O3	2b	¼	¾	½	4.2(2)	1[c]
Cu	2a	¼	¾	0	1.57(3)	0.98(1)
S	2c	¼	¼	0.07327(9)	1.01(4)	1[c]

[a] Inversion center located at (0, 0, 0): origin choice 2. [b] U(eq) is defined as one-third of the orthogonalized U_{ij} tensor. [c] Not refined. [d] Site restrained to be fully occupied.

single-crystal structure solution by the Patterson method in space group $P4$. The ADDSYM software implemented within PLATON[16] indicated that the actual space group was $P4/nmm$, and refinement of the model in this space group produced a refined formulation for the compound of $Ba_{1.32(3)}Sr_{0.68(4)}Mn_2O_4Cu_{0.98(2)}S$, fairly consistent with the EDX results, and confirmed that the compound adopts a new structure type. The refinement results are given in Table 1 and the refined atomic parameters are given in Table 2. We refer to this compound as $Ba_{1.3}Sr_{0.7}Mn_2O_4CuS$. This result resolved the observation that if a reaction mixture intended to produce $Ba_4Mn_3O_{7.5}Cu_2S_2$ (see refs 2,8) was cooled rapidly from a soak temperature of 900 °C (i.e., by removal from the furnace at 900 °C), then this target was obtained.[15] However, fairly slow (5 °C min^{-1}) cooling from 900 °C produced a product with a PXRD pattern that was inconsistent with this target. Instead, the $x = 0$ member of the $Ba_{2-x}Sr_xMn_2O_4Cu_{1-\delta}S$ series with the new structure identified from the SXRD measurements on $Ba_{1.3}Sr_{0.7}Mn_2O_4CuS$ was the majority phase produced under the slow cooling regime. Material of this new phase with target composition "$Ba_2Mn_2O_4CuS$" was subsequently synthesized free of the competing phase $Ba_4Mn_3O_{7.5}Cu_2S_2$ (as judged by laboratory PXRD analysis) as described in the Experimental Section.

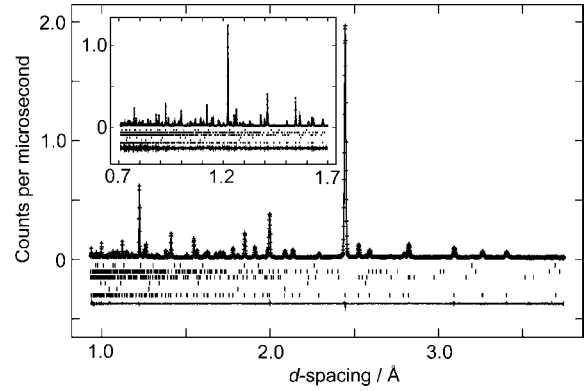

Figure 1. Results of Rietveld refinement of the structure of $Ba_2Mn_2O_4Cu_{0.9}S$ (sample A) against HRPD data. The diffractogram collected by the 90° detector bank is shown with that from the higher-resolution 163° detector bank shown in the inset. The data (points), fit (line) and difference plots (lower line) are shown. The reflection positions for the phases used in the refinement are indicated. From bottom: $Ba_2Mn_2O_4Cu_{0.89(1)}S$ (85.2 mol %; note that this phase constitutes 97% of the mass of the sample), Cu (9.4 mol%), MnO (1.9 mol %), $Ba_4Mn_3O_{7.5}Cu_2S_2$ (0.1 mol%), $BaCO_3$ (1.6 mol %), and BaS (1.8 mol%). The d-spacing region from 2.5 to 3.5 Å is shown enlarged in Figure S4 in the Supporting Information, and the region from 4 to 7 Å is shown in Figure 6.

Lattice parameters of $a = 3.9916(1)$ Å and $c = 19.5628(5)$ Å were obtained from Rietveld refinement against PXRD data using the model obtained from the SXRD analysis of $Ba_{1.3}Sr_{0.7}Mn_2O_4CuS$. Subsequent refinement against PND data collected on material of composition "$Ba_2Mn_2O_4CuS$" (sample A) using HRPD (see Figure 1) revealed small quantities of impurity phases: elemental Cu, 1.2 mass % (9.4 mol%); $Ba_4Mn_3O_{7.5}Cu_2S_2$,[15] 0.3 mass % (0.1 mol%); MnO, 0.3 mass% (1.9 mol %); BaS, 0.6 mass% (1.8 mol %) and $BaCO_3$ (derived from aerial carbonation of BaO): 0.7 mass % (1.6 mol %). These impurities fully accounted for all the Bragg reflections in the room-temperature PND pattern. The PND refinement results revealed that when the compound is strontium-free, the composition of the new oxysulfide phase is $Ba_2Mn_2O_4Cu_{0.89(1)}S$, with a substantial intrinsic copper deficiency that is discussed further below. We refer to this material as $Ba_2Mn_2O_4Cu_{0.9}S$. The SXRD results on strontium-containing material merely suggested a slight

(16) Fletcher, D. A.; McMeeking, R. F.; Parkin, D. *J. Chem. Inf. Comput. Sci.* **1996**, *36*, 746.

Table 3. Refined Atomic Positions for $Ba_2Mn_2O_4Cu_{0.9}S$ (sample A) in *P4nmm*[a] from PND Data Collected on HRPD at 298 K

atom	site	*x*	*y*	*z*	(U(eq)[b] (Å^2) × 100	occupancy
Mn1	2*c*	¼	¼	0.46755(4)	1.07(5)	1[c]
Mn2	2*c*	¼	¼	0.25989(6)	0.99(5)	1[c]
Ba1	2*c*	¾	¾	0.35154(5)	1.18(5)	1[c]
Ba2	2*c*	¾	¾	0.15526(3)	1.06(5)	1[c]
O1	4*f*	¼	¾	0.24624(3)	1.67(4)	1[c]
O2	2*c*	¼	¼	0.36499(4)	1.73(4)	1[c]
O3	2*b*	¼	¾	½	3.60(5)	1[c]
Cu	2*a*	¼	¾	0	2.21(4)	0.899(2)
S	2*c*	¼	¼	0.07123(8)	1.30(8)	1[c]

[a] Inversion center located at (0, 0, 0): origin choice 2. [b] U(eq) is defined as one-third of the orthogonalized U_{ij} tensor. [c] Not refined.

(~2%) copper deficiency that was on the same order as the uncertainty in the composition obtained by the SXRD refinement. The refinement results and the refined atomic parameters for $Ba_2Mn_2O_4Cu_{0.9}S$ are given in Tables 1 and 3, respectively. We have not yet been able to produce phase pure strontium-containing members, $Ba_{2-x}Sr_xMn_2O_4Cu_{1-\delta}S$. Evidently, there is strong competition between compounds with the new structure type and phases of fairly similar overall composition with the $Sr_4Mn_3O_{7.5}Cu_2S_2$[3] structure type, and samples containing both phases were invariably obtained.

The crystal structure of $Ba_2Mn_2O_4Cu_{0.9}S$ obtained from the room temperature PND refinement is shown in Figure 2. Bond lengths and angles for this phase at room temperature and for $Ba_{1.3}Sr_{0.7}Mn_2O_4CuS$ at 240 K are listed in Table 4.

Structural Comparisons. This new structure is related to that of $Sr_4Mn_3O_{7.5}Cu_2S_2$ as shown in Figure 2. The structure of $Sr_4Mn_3O_{7.5}Cu_2S_2$[3,9] consists of strontium manganite perovskite blocks, separated by Cu_2S_2 layers. The manganite blocks are similar to those that occur in the n = 3 Ruddlesden–Popper phases ($A_{n+1}M_nO_{3n+1}$), as discussed in the introduction and shown in ref 8.The structure of $Ba_2Mn_2O_4Cu_{0.9}S$ contains similar Cu_2S_2 layers, but the oxide blocks are quite different. Formally, the manganite layer in $Ba_2Mn_2O_4Cu_{0.9}S$ is related to that in $Sr_4Mn_3O_{7.5}Cu_2S_2$[3,9] in the following way: the central layer of MnO_6 octahedra in the manganite layer in $Sr_4Mn_3O_{7.5}Cu_2S_2$ is cleaved in the central MnO_2 plane. Termination of the cleavage plane yields two layers of square-based MnO_5 pyramidal units with their square bases facing each other across the cleavage plane. A basal-plane translation of (½, ½) (i.e., analogous to an *n*-glide plane) is then applied to one layer of MnO_5 pyramids relative to the other. The layers of MnO_5 pyramids are then rejoined so that each shares its four basal edges with MnO_5 pyramids from the other side of the original cleavage plane. The resulting manganite slab in $Ba_2Mn_2O_4Cu_{0.9}S$ is composed purely of four layers of MnO_5 square-based pyramids. Those in the central two layers share all their basal edges as described above and share their apical vertexes with those of MnO_5 pyramids in the outer layers of the slab. The pyramids in the outer layers of the slab in turn share all four basal vertexes with neighbors in the same layer. In the structures of both $Sr_4Mn_3O_{7.5}Cu_2S_2$[3,9] and $Ba_2Mn_2O_4Cu_{0.9}S$, alkaline earth cations occupy sites 12-coordinate by oxide that are similar to those occupied by the *A* cations in cubic perovskites, and they occupy further sites, analogous to those in the rock-salt layers of R−P phases, that are coordinated by four oxide and four sulfide ions in a distorted square antiprismatic arrangement. Compositionally, the two structure types are related by the insertion of an additional manganese ion into the central MnO_2 sheet in the $Sr_4Mn_3O_{7.5}Cu_2S_2$ structure (which has the ideal composition $Sr_4Mn_3O_8Cu_2S_2$ but is always found to be oxide deficient).[3,9,16] This leads to the formation of a puckered sheet of composition Mn_2O_2, which might be compared with a highly compressed fragment of the fluorite structure (i.e., with highly distorted edge-shared OMn_4 tetrahedra) and has previously been compared[10] with a highly puckered (1 0 0) plane of the rock salt structure. To the best of our knowledge, this metalate motif has not been observed previously in relatives of the Ruddlesden–Popper oxides. However, the relationship between the structures of the oxide slabs of $Sr_4Mn_3O_{7.5}Cu_2S_2$[3] and $Ba_2Mn_2O_4Cu_{0.9}S$ mirrors the formal relationship between the perovskite $SrFeO_3$[18] and the idealized structure of $Sr_4Fe_6O_{12}$, the oxide-poor analogue of the complex $Sr_4Fe_6O_{13\pm\delta}$ phases. The idealized structure of $Sr_4Fe_6O_{12}$ (= $Sr_2Fe_3O_6$) discussed in ref would be obtained from the cubic perovskite $SrFeO_3$ (= $Sr_2Fe_2O_6$) by the insertion of a double layer of basal-edge-sharing FeO_5 square pyramids in place of alternate layers of FeO_6 octahedra. Furthermore, the structures of $BaNiS_2$,[19] one polymorph of $BaCoS_2$,[20] $KCoO_2$,[21] and the nitrides AMN_2 (A = Sr, M = Ti;[22] A = Ba, M = Zr,[23] Hf)[24] are related to the common K_2NiF_4 n = 1 Ruddlesden–Popper structure by the formal replacement of all the layers of metalate octahedra by double layers of basal-edge-sharing metalate square-based pyramids. The relationships between the frameworks composed of the transition metal and anions in various structures containing edge-linked five-vertex polyhedra are shown in Figure 3. $Bi_4Sr_{14}Fe_{24}O_{56}$, a relative of $Sr_4Fe_6O_{13}$, has recently been identified.[25]

The refinements against SXRD and PND data reveal well-behaved anisotropic displacement ellipsoids for all atoms apart from O3, the anion in the center of the oxide slab involved in edge-sharing of MnO_5 square pyramids. This anion has an ellipsoid that is extremely elongated in the *c* direction: U_{33}/U_{11} = 5.6 for $Ba_{1.3}Sr_{0.7}Mn_2O_4CuS$ at 240 K from SXRD and 7.1 for $Ba_2Mn_2O_4Cu_{0.9}S$ at 298 K from PND. The anisotropy increases with decreasing temperature for $Ba_2Mn_2O_4Cu_{0.9}S$ with U_{33} for O3 diminishing by only 17% between 298 and 2 K, compared with decreases of 50−90% for the parameters of the better behaved ellipsoids, indicating that this ellipsoid is not merely thermal in nature. There was no indication from the refinements against PND data of any deficiency on the anion sites in Ba2Mn2O4Cu0.9S.

(17) Spek, A. L. *J. Appl. Crystallogr.* **2003**, *36*, 7.
(18) Hodges, J. P.; Short, S.; Jorgensen, J. D.; Xiong, X.; Dabrowski, B.; Mini, S. M.; Kimball, C. W. *J. Solid State Chem.* **2000**, *151*, 190.
(19) Grey, I. E.; Steinfink, H. *J. Am. Chem. Soc.* **1970**, *92*, 5093.
(20) Gelabert, M. C.; Brese, N. E.; DiSalvo, F. J.; Jobic, S.; Deniard, P.; Brec, R. *J. Solid State Chem.* **1996**, *127*, 211.
(21) Jansen, M.; Hoppe, R. *Z. Anorg. Allg. Chem.* **1975**, *417*, 31.
(22) Gregory, D. H.; Barker, M. G.; Edwards, P. P.; Siddons, D. J. *Inorg. Chem.* **1998**, *37*, 3775.
(23) Seeger, O.; Hofmann, M.; Straehle, J. *Z. Anorg. Allg. Chem.* **1994**, *620*, 2008.
(24) Gregory, D. H.; Barker, M. G.; Edwards, P. P.; Slaski, M.; Siddons, D. J. *J. Solid State Chem.* **1998**, *137*, 62.
(25) Lepoittevin, C.; Malo, S.; Hervieu, M.; Grebille, D.; Raveau, B. *Chem. Mater.* **2004**, *16*, 5731.
(26) Sander, K.; Müller-Buschbaum, H. *Z. Anorg. Allg. Chem.* **1979**, *451*, 35.

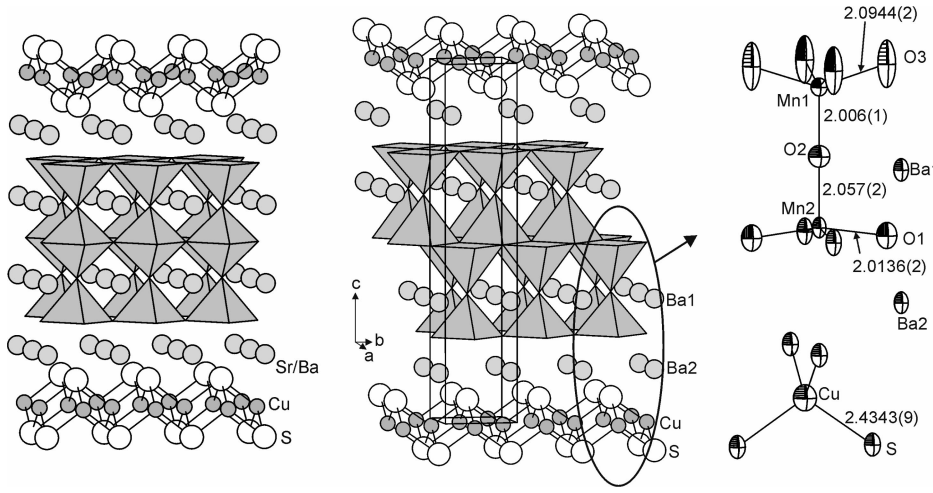

Figure 2. Crystal structure of $Ba_2Mn_2O_4Cu_{0.9}S$ (center) with MnO_5 square-based pyramids shown as polyhedra and the other atoms shown as spheres. The enlarged region at right shows the asymmetric unit and the coordination environments of the Mn and Cu ions. Displacement ellipsoids derived from the refinement against HRPD data at room temperature are shown at the 75% level, and selected bond lengths are given in Å. The left-hand diagram shows an equivalent portion of the idealized structure of $A_4Mn_3O_{8-\delta}Cu_2Ch_2$ (A = Sr, Ba; Ch = S, Se; $\delta \approx 0.5$)[2,8,15] for comparison.

Table 4. Selected Bond Lengths (Å) and Angles (deg)

	$Ba_2Mn_2O_4Cu_{0.9}S$ (sample A)	$Ba_{1.3}Sr_{0.7}Mn_2O_4CuS$
T (K)	298	240
Mn1−O2 [1][a]	2.007(1)	2.008(5)
Mn1−O3 [4]	2.0945(2)	2.0828(3)
<Mn1−O>[b]	2.077	2.068
Mn2−O2 [1]	2.056(2)	2.071(5)
Mn2−O1 [4]	2.0137(2)	1.9947(4)
<Mn2−O>[b]	2.022	2.010
Cu−S [4]	2.4342(9)	2.430(1)
O2−Mn1−O3 [4]	107.65(2)	108.10(3)
O3−Mn1−O3 [4]	84.73(1)	84.46(2)
O3−Mn1−O3 [2]	144.71(4)	143.79(6)
O2−Mn2−O1 [4]	97.62(4)	97.0(1)
O1−Mn2−O1 [4]	88.99(1)	89.15(2)
O1−Mn2−O1 [2]	164.77(8)	166.0(2)
S−Cu−S [4]	109.13(3)	109.63(3)
S−Cu−S [2]	110.16(6)	109.15(7)

[a] The numbers in square brackets indicate the number of bonds or angles of a particular type. [b] Weighted average bond length.

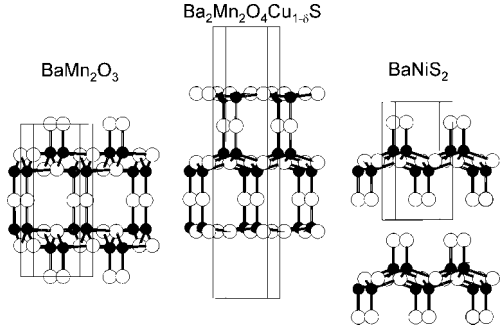

Figure 3. Comparison of the structures of frameworks described by linking MX_5 polyhedra via edges and vertexes. The MX_2 layers first identified in $BaNiS_2$[19] (right) resemble the central portion of the manganese oxide layer in the title compound (center). Part of the framework in $BaMn_2O_3$[26] (left) has a similar topology, but in this compound, the square-based pyramids are replaced by distorted triangular bipyramids, leading to a distortion from tetragonal symmetry.

U_{33}/U_{11} for O3 assumes a very large value of ~ 200 at 2 K. which is probably partly an artifact of the refinement; a similar degree of anisotropy is suggested in the refinement from SXRD data of $BaZrN_2$,[24] which is reported with a large U_{33} and an unphysical (negative) U_{11} for the anisotropic ellipsoid of the N atom involved in edge-sharing of ZrN_5 square pyramids, presumably as a consequence of the high anisotropy in this light atom. Refinements of the oxysulfide structures using a split site model with the O3 atom located at (¼ ¾ ½ ± ϵ) and with the two components of the split site each half-occupied in a disordered fashion were unsuccessful in the case of the refinement of $Ba_{1.3}Sr_{0.7}Mn_2O_4CuS$ against SXRD data (a residual electron density peak of 3 e $Å^{-3}$ remained at the ideal position, and R_1 increased from 0.0214 to 0.0258), but in the cases of $Ba_2Mn_2O_4Cu_{0.9}S$, the model refined satisfactorily against PND data, although with no improvement in the agreement factors. δ refined to 0.0121(1) at 298 K, i.e., the split positions were separated by 0.47 Å. The interpretation of the elongated ellipsoids and the split site model is that locally the square pyramids are distorted from C_{4v} symmetry, but the orientation of this distortion is disordered on the length scale probed by diffraction methods. A contrast is provided by the orthorhombic crystal structure of $BaMn_2O_3$.[26] This contains a network of MnO_5 polyhedra shown in Figure 3 which are linked by sharing four of their edges and the remaining vertex, just like the Mn1-centered MnO_5 square-based pyramids in $Ba_2Mn_2O_4Cu_{0.9}S$. The MnO_5 units in $BaMn_2O_3$ are derived from square-based pyramids by puckering the square base as shown in Figure 3 so as to lower the symmetry to C_{2v} and form polyhedra that are best described as distorted triangular bipyramids. This is an example of an orientationally ordered distortion of an edge-linked network of square-based pyramids and results in a large distortion from tetragonal symmetry.

Cu Deficiency and Mn Oxidation States. A refined composition of $Ba_2Mn_2O_4Cu_{0.899(2)}S$ was obtained in the refinement against PND data collected for sample A on HRPD at 298 K. A further refinement of the structure of the sample A measured on the POLARIS diffractometer at ISIS, which has the advantage over HRPD of coverage of a wider range of d-spacings, produced a composition of $Ba_2Mn_2O_4Cu_{0.871(2)}S$. Given the uncertainties inherent in determining site occupancies from powder diffraction data (the esds determined by GSAS in these refinements are

almost certainly unrealistically small), we deduce that a composition of $Ba_2Mn_2O_4Cu_{0.89(1)}S$ is reasonable. Elemental copper was identified in the patterns as described above and the average of the refined ratios of the phase fractions of $Ba_2Mn_2O_4Cu_{0.89(1)}S$ and elemental Cu obtained from HRPD and POLARIS data of 1:0.11(1) is entirely consistent with the observed copper deficiency (i.e., the PND measurements, which probe the entire sample, provide two independent and consistent measures for the copper deficiency in $Ba_2Mn_2O_4Cu_{0.89(1)}S$, so we can be sure that the less-than-full Cu site occupancy is not simply an artifact of the refinements). Such copper deficiency has been observed previously in related compounds (the series $Sr_2MnO_2Cu_{2m-\delta}S_{m+1}$,[5] $Sr_2CoO_2Cu_{2-\delta}S_2$,[3] and $CeOCu_{1-\delta}S$[27]), and it seems that the copper occupancy in these oxychalcogenides is the variable that optimizes the electron count according to the demands of the transition metal in the oxide layer. Subsequently, a second sample (sample B) entirely free of elemental copper according to PXRD measurements (Figure S1, Supporting Information) and containing low levels of MnO, BaS, and $BaCO_3$ impurities similar to those in the sample used in the PND investigations was obtained with a composition of $Ba_2Mn_2O_4Cu_{0.9}S$ (i.e., equal within uncertainty to the composition derived from the PND measurements).

The compositions of the phases suggest an almost equal population of the two distinct and equally abundant Mn sites by Mn^{2+} and Mn^{3+} ions. The layers of Mn2-centered MnO_5 square pyramids on the outside of the manganite slabs share only their vertexes with other MnO_5 polyhedra. In $Ba_2Mn_2O_4Cu_{0.9}S$, the four basal Mn2−O distances in these polyhedra are 2.0136(2) Å and the apical bond length is 2.057(2) Å (mean of 2.022 Å). The MnO_5 square pyramids in the center of the manganite slab share basal edges with each other, resulting in Mn−Mn approaches of 3.095 Å. The Mn1−O distances in these MnO_5 pyramids using an unsplit O3 site are 2.0944(2) Å (basal) and 2.006(1) Å (apical) (on average 2.077 Å), slightly longer distances than are found in the MnO_5 pyramids on the outside of the manganate slabs. These distances and those in $Ba_{1.3}Sr_{0.7}Mn_2O_4CuS$ are summarized in Table 4. Note that if the split O3 model is employed for $Ba_2Mn_2O_4Cu_{0.9}S$ the mean Mn1−O distance increases to 2.087 Å, which should perhaps be viewed as a more realistic description of the local situation. The longer mean Mn−O distance in the "inner" MnO_5 square pyramids in the center of the oxide slab and the need to accommodate a relatively short Mn−Mn approach across edges shared by these polyhedra suggests that the "outer" MnO_5 square pyramids may be populated predominantly by Mn^{3+} ions, whereas the inner square pyramids are populated predominantly by Mn^{2+} ions. In considering the extent of such charge ordering, comparisons with related systems are helpful: the defect perovskite $YBaMn_2O_5$[28] also contains MnO_5 square pyramids that form layers through sharing of basal vertexes, and these layers are joined to form double layers through sharing of the remaining apical vertexes. Structural and magnetic analysis reveals in this case complete charge ordering of Mn^{2+} and Mn^{3+} sites, and the mean Mn−O distances around each Mn ion are 2.068 Å for Mn^{2+} and 1.943 Å for Mn^{3+}, a larger difference in mean bond lengths than is found in our case. Other compounds containing Mn^{3+} ions in square pyramidal coordination include $Sr_2Mn_2O_5$[27] and $Ca_2Mn_2O_5$[30] with mean Mn−O distances of 1.955 and 1.921 Å, respectively. The oxysulfide compounds $A_4Mn_3O_{7.5}Cu_2S_2$ (A = Sr, Ba)[3,9,16] (see Figure 2) contain Mn^{3+} ions in a square pyramidal environment closely similar to that of the Mn2 ions in the outer portions of the oxide slabs described in $Ba_2Mn_2O_4Cu_{0.9}S$. For $Sr_4Mn_3O_{7.5}Cu_2S_2$,[3,9] the mean Mn−O distance is 1.961 Å, similar to the distances in $YBaMn_2O_5$ and $Sr_2Mn_2O_5$.

Bond valence calculations carried out using the EUTAX package[31] show that in $Sr_4Mn_3O_{7.5}Cu_2S_2$[9] the calculated bond valence sum (BVS) for square pyramidal Mn^{3+} is 2.95. For $Ba_4Mn_3O_{7.5}Cu_2S_2$,[16] the mean Mn−O distance is significantly longer than in the strontium analogue at 2.046 Å and is similar to that in $Ba_2Mn_2O_4Cu_{0.9}S$. In $Ba_4Mn_3O_{7.5}Cu_2S_2$[16] and $Ba_2Mn_2O_4Cu_{0.9}S$, the BVS for Mn^{3+} ions in the corresponding square pyramidal sites in the outer parts of the oxide slabs are 2.32 and 2.46, respectively, showing that Mn^{3+} is extremely underbonded when a large cation is accommodated in the manganese oxide framework. Such large deviations of the bond valence sum from the expected value are a feature of crystal structures with relatively few structural variables.[32] For example, in the isostructural Ruddlesden–Popper Mn^{4+} phases $Sr_3Mn_2O_7$[33] and $Ca_3Mn_2O_7$,[34] the bond valence sums for Mn show slight underbonding in the case of $Sr_3Mn_2O_7$ (BVS = 3.84) and substantial overbonding in the case of $Ca_3Mn_2O_7$ (BVS = 4.42). In $Ba_2Mn_2O_4Cu_{0.9}S$, the BVS for the Mn1 site in the central part of the layer and deemed to be occupied by Mn^{2+}, is 2.31 indicating overbonding. The Madelung potentials at the Mn1 and Mn2 sites were also more similar (−30.81 V for the Mn1 site and −32.99 V for the Mn2 site) than would be expected if Mn1 were exclusively occupied by Mn^{2+}, and Mn2 by Mn^{3+}. These calculations and comparisons of the bond lengths in $Ba_2Mn_2O_4Cu_{0.9}S$ with those in related compounds suggest that the underbonding of a Mn^{3+} ion on the Mn2 site and the overbonding of a Mn^{2+} ion on the Mn1 site might be relieved by disordering of the Mn^{2+} and Mn^{3+} states over the two available sites, although it would be expected that this tendency for Mn^{3+} to occupy the smaller Mn1 site in the central part of the slab would be resisted by coulombic Mn−Mn repulsion across the shared edges of these MnO_5 square pyramids. Furthermore, in $Ba_2Mn_2O_4Cu_{0.9}S$, the copper deficiency suggests partial oxidation of Mn^{2+} to give

(27) Chan, G. H.; Deng, B.; Bertoni, M.; Ireland, J. R.; Hersam, M. C.; Mason, T. O.; Van Duyne, R. P.; Ibers, J. A. *Inorg. Chem.* **2006**, *45*, 8264.

(28) Millange, F.; Suard, E.; Caignaert, V.; Raveau, B. *Mater. Res. Bull.* **1999**, *34*, 1.

(29) Caignaert, V.; Nguyen, N.; Hervieu, M.; Raveau, B. *Mater. Res. Bull.* **1985**, *20*, 479.

(30) Poeppelmeier, K. R.; Leonowicz, M. E.; Longo, J. M. *J. Solid State Chem.* **1982**, *44*, 89.

(31) Brese, N. E.; O'Keeffe, M. *Acta Crystallogr., Sect. B* **1991**, *47*, 192.

(32) Brown, I. D. The Chemical Bond in Inorganic Chemistry. In *The Bond Valence Model IUCr Monograph on Crystallography 12*; Oxford University Press: Oxford, U.K., 2002.

(33) Mitchell, J. F.; Millburn, J. E.; Medarde, M.; Short, S.; Jorgensen, J. D.; Fernandez-Diaz, M. T. *J. Solid State Chem.* **1998**, *141*, 599.

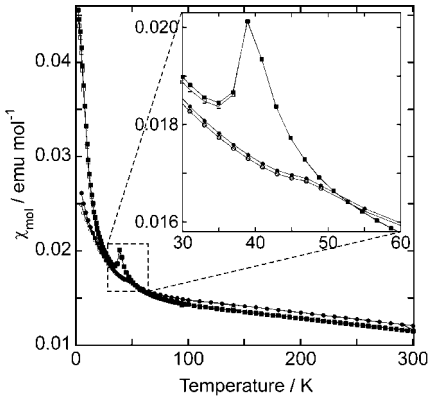

Figure 4. Magnetic susceptibilities of $Ba_2Mn_2O_4Cu_{0.9}S$ samples measured under zero-field-cooled (ZFC) and field-cooled (FC) conditions in a measuring field of 0.1 T. The inset shows the maxima in the susceptibility described in the text. Key: Sample A ZFC (□) and FC (■); sample B ZFC (○) and FC (●).

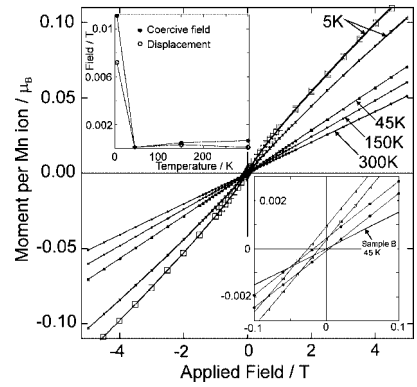

Figure 5. Magnetization isotherms for $Ba_2Mn_2O_4Cu_{0.9}S$. The main figure shows the isotherms for sample A at 5 K (□) and for the copper-free sample B at several temperatures. The lower right inset compares the small hysteresis and displacement from the origin for samples A (□) and B (○) at 5 K (the isotherm for sample B at 45 K that shows almost negligible hysteresis and displacement is also shown for comparison). The upper left inset shows the variation with temperature of the coercive field and displacement from the origin of the isotherms for sample B. The lines joining the points are guides for the eye.

a mean Mn oxidation state of +2.55, which makes incomplete partitioning of the oxidation states inevitable.

Electrical Conductivity Measurements. Electrical conductivity measurements carried out using a four-probe set up using a homemade apparatus on sample B made with a composition $Ba_2Mn_2O_4Cu_{0.9}S$ and containing no elemental copper revealed that the compound has a high resistivity of 2.5×10^6 Ω cm at room temperature and the resistance could not be reliably measured below 190 K (Figure S3, Supporting Information). The temperature dependence shows the material to be semiconducting.

Magnetic Properties. Magnetometry measurements were carried out on samples A and B containing the phase $Ba_2Mn_2O_4Cu_{0.9}S$. Measurements were performed under ZFC and FC conditions in a measuring field of 0.1 T and are shown in Figure 4. The measurements on sample A (the sample used for PND measurements) revealed the presence of a sharp cusp in the magnetic susceptibility at 40 K and the ZFC and FC curves were coincident above this temperature. However, at lower temperatures, the susceptibility continues to rise and the FC and ZFC curves diverge slightly, suggesting that the compound shows spin-glass-like behavior. Similar measurements on sample B (the copper-free sample used for conductivity measurements) showed a broader maximum in the susceptibility at 45 K and similar divergence of the FC and ZFC curves. The susceptibilities of the two samples are qualitatively similar, although the differences around 40–50 K suggest that they may have slightly different compositions close to $Ba_2Mn_2O_4Cu_{0.9}S$. The inverse susceptibilities appear to show a linear variation with temperature at close to room temperature, the suggested Weiss constants obtained by extrapolation to $1/\chi = 0$ were about −650 K which indicates that the Curie–Weiss law is not applicable in the temperature regime studied. Magnetization isotherms of the two samples measured at 5 K (Figure 5) showed a slight hysteresis (coercive field of 0.0156(2) T for sample A and 0.0111(2) T for sample B) in the magnetization of the sample and the isotherms was displaced by from the origin by −0.0178(2) T (sample A) and −0.0072(2) T (sample B) after cooling in an applied field of +5 T. These observations support the conclusion that the material shows spin-glass-like behavior. Magnetization isotherms measured on sample B at 45, 150, and 300 K showed that around the transition temperature identified at 45 K from the susceptibility plot, the coercive field and the displacement of the isotherms from the origin are on the order of only 0.0001 T, values that increase slightly at higher temperatures as shown in the inset to Figure 5. It should be noted that the plot of sample magnetization against applied magnetic field at 300 K for sample B is linear and there is no indication of any adventitious ferromagnetic impurity that could result in the observed divergence of the FC and ZFC curves. Furthermore, the observation of hysteresis and displacement of the magnetization isotherms obtained after high-field cooling are diagnostic of spin-glass-type behavior. The 0.3% by mass impurities of antiferromagnetic MnO ($T_N \sim 115$ K) account for about 1% of the magnetic moment of the sample according to the reported behavior of MnO.[35]

A PND measurement carried out on HRPD at 2 K on sample A revealed that the main features of the structure of $Ba_2Mn_2O_4Cu_{0.9}S$ were unchanged on cooling, with no lowering of symmetry evident on HRPD. However, additional reflections were observed at long *d*-spacings, mainly in the 30° bank, which has a fairly poor signal-to-noise ratio (Figure 6). It was not possible to index all of these reflections on simple expansions of the nuclear unit cell. However, a subset of the magnetic reflections was modeled satisfactorily (Figure 6) using an ordered magnetic model in which just the moments on the Mn2 sites in the outer parts of the manganese oxide slab were coupled antiferromagnetically to their four Mn2 nearest neighbors and aligned along the crystallographic *c* axis, similar to the model used in $Sr_4Mn_3O_{7.5}Cu_2$ Ch_2 (Ch = S, Se).[9] This magnetic unit cell had dimensions $\sqrt{2}a \times \sqrt{2}a \times c$, where a and c are the dimensions of the nuclear cell and the refined moment per Mn2 ion was 2.3(1) μ_B, much smaller than the expected value of the spin only moment of 4 μ_B for Mn^{3+} ions, even

(34) Lobanov, M. V.; Greenblatt, M.; Caspi, E. N.; Jorgensen, J. D.; Sheptyakov, D. V.; Toby, B. H.; Botez, C. E.; Stephens, P. W. *J. Phys.: Condens. Matter* **2004**, *16*, 5339.
(35) Tyler, R. W. *Phys. Rev.* **1933**, *44*, 776.

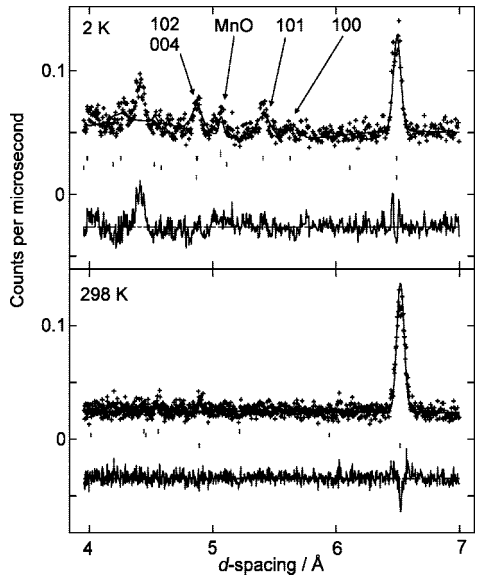

Figure 6. Comparison of the PND patterns for $Ba_2Mn_2O_4Cu_{0.9}S$ (sample A) measured at 298 K (lower) and 2 K (upper) using the HRPD 30° bank, showing the appearance of peaks due to magnetic scattering at 2 K. Miller indices for the cell of a magnetic structure with cell dimensions $\sqrt{2}a \times \sqrt{2}a \times c$ relative to the nuclear cell and with only Mn2 ions carrying an ordered moment of 2.3(1) μ_B oriented along the z direction indicated, along with the magnetic 003 reflection for MnO.[36] Further magnetic peaks remain unindexed (see Figure S4 in the Supporting Information). Symbols are as defined in the caption to Figure 1.

allowing for a reduction expected from covalent bonding. A further magnetic reflection at 5.07 Å was identified as the 003 reflection from the magnetic structure of MnO.[36] The remaining magnetic reflections, which were not accommodated using this model, had a total integrated intensity approximately equal to that of the magnetic reflections that were modeled successfully and were also somewhat broader. It is plausible that the additional reflections arise from a second magnetic phase that is present in this compound, because the only impurity phase, aside from MnO, that can show magnetic scattering is $Ba_4Mn_3O_{7.5}Cu_2S_2$,[15] present at the level of about 0.2 mol % compared with the main phase. It is important to emphasize that the current data do not allow us to come to any firm conclusions regarding the origin of any of the magnetic scattering, but at the very least, this analysis, in which a plausible model accounts quantitatively for about half of the magnetic scattering intensity, shows that the total intensity of the magnetic scattering is significantly less than what would be expected if all the Mn spins from d^5 Mn^{2+} ions and d^4 Mn^{3+} ions on the Mn1 and Mn2 sites were to participate in long-range magnetic ordering. This is consistent with the observation of spin-glass behavior, which presumably arises from spins that do not participate in magnetic ordering.

The observation of spin-glass character implies that the system is inherently frustrated and disordered. The competing 90° ferromagnetic and 180° antiferromagnetic superexchange interactions expected[37,38] between Mn1 ions in the edge-sharing polyhedra in the central layer of the Manganite slab can provide frustration, and as noted above, disorder of the Mn^{2+} and Mn^{3+} ions over the available pyramidal sites might relieve some strain in the system. Furthermore, the Cu deficiency implies partial oxidation of Mn to the +2.55 oxidation state, which must introduce some chemical disorder. However, further investigations are required to fully account for the magnetic behavior of this compound.

Conclusions

We have synthesized examples of a new layered oxysulfide containing a perovskite-related alkaline earth manganese oxide slab composed purely of edge- and vertex-sharing MnO_5 square-based pyramids. This structural fragment has not, to the best of our knowledge, been reported previously in an oxide, although it is closely emulated in the complex structures of compounds $Sr_4Fe_6O_{13\pm\delta}$ and shares features with other transition metal oxide, sulfide, and nitride compounds that contain layers of edge-sharing square-based pyramids. Disorder, which may result from incomplete charge ordering between Mn^{2+} and Mn^{3+} states, and the intrinsic frustration of the superexchange interactions within the central part of the oxide slab can account for spin-glass behavior, although the appearance of magnetic Bragg reflections shows that some of the Mn moments are involved in long-range magnetic order.

Acknowledgment. We thank Dr R. M. Ibberson, ISIS facility, for assistance with the neutron diffraction investigations, Dr. Norman Charnley, Department of Earth Sciences, University of Oxford, for assistance with EDX analysis. We thank the EPSRC for the award of studentships for G.H. and C.F.S., for access to the ISIS facility and for access to the Chemical Database Service at Daresbury.

Supporting Information Available: Crystallographic data in CIF format for $Ba_{1.3}Sr_{0.7}Mn_2O_4CuS$ (240 K). Table of refined atomic coordinates at 2 K for $Ba_2Mn_2O_4Cu_{0.9}S$ (from sample A; Table S1); diagrams showing PXRD pattern for the sample of $Ba_2Mn_2O_4Cu_{0.9}S$ (sample B) used in electrical resistivity measurements (Figure S1), Rietveld fits against PND data at 2 K for $Ba_2Mn_2O_4Cu_{0.9}S$ (sample A; Figure S2), electrical resistivity of $Ba_2Mn_2O_4Cu_{0.9}S$ (sample B; Figure S3), magnetic scattering of $Ba_2Mn_2O_4Cu_{0.9}S$ (sample A; Figure S4) (PDF). This material is available free of charge via the Internet at http://pubs.acs.org.

CM7021054

(36) Goodwin, A. L.; Tucker, M. G.; Dove, M. T.; Keen, D. A. *Phys. Rev. Lett.* **2006**, *96*, 047209.
(37) Goodenough, J. B. *J. Phys. Chem. Solids* **1958**, *6*, 287.
(38) Kanamori, J. *J. Phys. Chem. Solids* **1959**, *10*, 87.